Engineering helical phase via four-wave mixing in the ultraslow propagation regime

Chao Yu and Zhiping Wang*

Information Materials and Intelligent Sensing Laboratory of Anhui Province, Anhui University, Hefei 230601, China and Key Laboratory of Opto-Electronic Information Acquisition and Manipulation of Ministry of Education, Anhui University, Hefei 230601, China

(Received 23 September 2020; revised 6 January 2021; accepted 7 January 2021; published 25 January 2021)

We describe a theoretical investigation of a four-wave mixing (FWM) scheme in a six-level atomic system driven by a field with orbital angular momentum and making use of two electromagnetically induced transparency (EIT) control fields. The obtained results allow us to control the helical phase of the output FWM field by varying the intensities of the two EIT control fields as well as the detuning of the probe field. More interestingly, we can achieve FWM output fields that are very stable under variation of the system parameters and allow the helical phase twist to be manipulated and suppressed, if desired, by adjusting the probe detuning. In this way, our scheme may open a tool to control the helical phase in a compact, efficient, and robust way.

DOI: 10.1103/PhysRevA.103.013518

I. INTRODUCTION

It is well known that the electromagnetically induced transparency (EIT) can modify the linear and nonlinear responses of the medium to the applied fields [1–3], which allows the optical properties of atomic media to be manipulated and hence leads to the suppression of the linear absorption and the enhancement of the nonlinear susceptibility. Using the EIT, the four-wave mixing (FWM) in the ultraslow propagation regime has been the focus of many scenarios. As examples, a highly efficient FWM experiment based on the EIT technique was performed in rubidium atomic vapor [4]. Deng *et al.* [5] demonstrated a novel channel-opening technique of FWM associated ultraslow propagation in a four-level system and showed that a new wave-mixing channel may be opened deep inside the medium, and the efficiency of the FWM can be significantly enhanced. Subsequently, ultraslow FWM resulting from multiphoton destructive interference [6] and double-dark resonances [7] have been proposed. Moreover, the coexistence of and interference between FWM and six-wave mixing processes in the EIT condition were observed in an inverted Y-type atomic system [8]. However, these studies are performed with space-independent laser beams without carrying orbital angular momentum (OAM).

The OAM light [9], unlike the conventional laser beam, represents a fundamentally new optical degree of freedom and provides unique optical properties [10]. Based on the OAM light, nonlinear FWM processes have been investigated [11–14] in recent decades. Unfortunately, in all these schemes the helical phase wave front of the FWM field is not fully controlled. Quite recently, we proposed some schemes to control the helical phase using FWM in atoms [15] or in semiconductor quantum wells [16,17]. It is interesting to note that the obtained results allow us to engineer the helical phase wave front via multiphoton quantum interference.

In this paper, we theoretically propose a scheme to manipulate the helical phase via ultraslow four-wave mixing in a six-level atomic system driven by a field with OAM and making use of two EIT control fields. Different from those previous studies, the distinguishing features of this scheme are given as follows: First and foremost, the helical phase profile can be modified in a controllable way that enhances or suppresses the phase twist by adjusting the detuning of the probe field or the intensities of the two EIT control fields. Second, the intensity distributions of the FWM field remain stable at different system parameters, showing the generated OAM mode stability. Third, this system is a double-dark resonance system [18,19] which has many advantages for controlling the FWM in comparison with the single EIT one. For instance, the double-dark resonance provides two transparency windows, and in different windows the spatial variations of the FWM are different. In this sense, the scheme allows us to explore singularity characteristics of the helical phase wave front based on nonlinear FWM processes, which may be useful in phase imprinting of Bose-Einstein condensates [20], atom manipulation with optical tweezers [21], and new structured-beam generation [22].

II. MODEL AND DYNAMIC EQUATIONS

We propose a six-level tripod system with three ground states ($|0\rangle$, $|4\rangle$, and $|5\rangle$) and three excited states ($|3\rangle$, $|2\rangle$, and $|1\rangle$), as shown in Fig. 1. A weak pulse probe field $\Omega_p = \Omega_{p0}\sqrt{\pi/(2\ln 2)}\exp[-t^2/(2\ln 2/\pi^2)]$ (t is the time and Ω_{p0} is a constant related to the value of the initial Rabi frequency at time $t = 0$) drives the transition $|0\rangle \rightarrow |3\rangle$. Two additional continuous-wave laser fields Ω_{c1} and Ω_{c2} form a tripod EIT configuration with states $|0\rangle$, $|3\rangle$, $|4\rangle$, and $|5\rangle$ and thus a dispersion modulation of state $|3\rangle$. The transitions $|3\rangle \rightarrow |2\rangle$ and $|2\rangle \rightarrow |1\rangle$ are coupled by a pump field Ω_a and a field

*Corresponding author: wzp@ahu.edu.cn

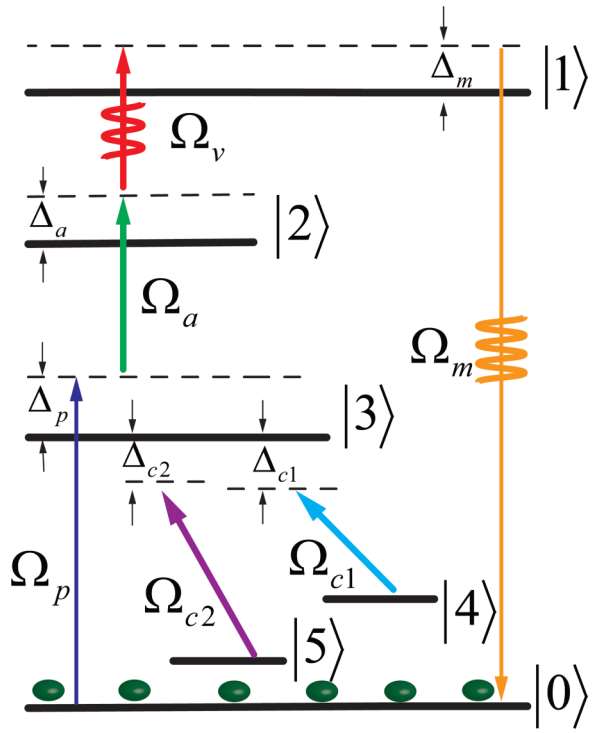

FIG. 1. Diagram of the six-level atomic system.

carrying OAM Ω_v, respectively. Here, the OAM field is a Laguerre-Gaussian mode and is given as

$$\Omega_v = \Omega_{v0}\Omega(r)e^{-il\phi}, \tag{1}$$

where $\Omega(r) = \frac{\sqrt{2p!/\pi(p+|l|)!}}{\omega_0}(\frac{\sqrt{2}r}{\omega_0})^{|l|}L_p^{|l|}(\frac{2r^2}{\omega_0^2})e^{-r^2/\omega_0^2}$, Ω_{v0} is the initial Rabi frequency of the LG field, r is the radius, and the beam waist is ω_0. ϕ is the azimuthal angle, and $L_p^{|l|}$ is the Laguerre polynomial. The radial index and azimuthal index are defined by p and l, respectively. It is expected that an internal FWM field Ω_m containing OAM information will be generated.

Based on the electric dipole and the rotating-wave approximations, the Hamiltonian in the interaction picture is given by ($\hbar = 1$)

$$\begin{aligned} H_I = {} & \Delta_m|1\rangle\langle 1| + \Delta_a|2\rangle\langle 2| + \Delta_p|3\rangle\langle 3| \\ & + (\Delta_p - \Delta_{c1})|4\rangle\langle 4| + (\Delta_p - \Delta_{c2})|5\rangle\langle 5| \\ & - (\Omega_p e^{i\mathbf{k}_p\cdot\hat{\mathbf{r}}}|3\rangle\langle 0| + \Omega_a e^{i\mathbf{k}_a\cdot\hat{\mathbf{r}}}|2\rangle\langle 3| \\ & + \Omega_v e^{i\mathbf{k}_v\cdot\hat{\mathbf{r}}}|1\rangle\langle 2| + \Omega_{c1}e^{i\mathbf{k}_{c1}\cdot\hat{\mathbf{r}}}|3\rangle\langle 4| \\ & + \Omega_{c2}e^{i\mathbf{k}_{c2}\cdot\hat{\mathbf{r}}}|3\rangle\langle 5| + \Omega_m e^{i\mathbf{k}_m\cdot\hat{\mathbf{r}}}|1\rangle\langle 0| + \text{H.c.}), \end{aligned} \tag{2}$$

where Δ_p, Δ_a, Δ_m, Δ_{c1}, and Δ_{c2} represent the detunings of the corresponding optical transitions. $\mathbf{k}_i$ ($i = p, a, v, m, c1, c2$) are wave vectors of the corresponding fields. $\hat{\mathbf{r}}$ is the position vector. Then the evolution equations for the probability amplitudes a_i ($i = 0$–5) can be easily obtained from Schrödinger's equation [23],

$$\frac{\partial a_1}{\partial t} = i\Omega_v a_2 + i\Omega_m a_0 + i(\Delta_m + i\gamma_1)a_1, \tag{3a}$$

$$\frac{\partial a_2}{\partial t} = i\Omega_v^* a_1 + i\Omega_a a_3 + i(\Delta_a + i\gamma_2)a_2, \tag{3b}$$

$$\begin{aligned} \frac{\partial a_3}{\partial t} = {} & i\Omega_a^* a_2 + i\Omega_p a_0 + i\Omega_{c2}a_5 \\ & + i\Omega_{c1}a_4 + i(\Delta_p + i\gamma_3)a_3, \end{aligned} \tag{3c}$$

$$\frac{\partial a_4}{\partial t} = i\Omega_{c1}^* a_3 + i(\Delta_p - \Delta_{c1} + i\gamma_4)a_4, \tag{3d}$$

$$\frac{\partial a_5}{\partial t} = i\Omega_{c2}^* a_3 + i(\Delta_p - \Delta_{c2} + i\gamma_5)a_5, \tag{3e}$$

where γ_i ($i = 1$–5) are the corresponding decay rates of the atomic state $|s\rangle$ ($s = 1$–5).

The propagations of the probe and FWM fields in the atomic medium are described by Maxwell's equations,

$$\frac{\partial\Omega_p}{\partial z} + \frac{\partial\Omega_p}{c\partial t} = \frac{ci}{2\omega_p}\nabla_\perp^2\Omega_p + ik_{03}a_3a_0^*, \tag{4a}$$

$$\frac{\partial\Omega_m}{\partial z} + \frac{\partial\Omega_m}{c\partial t} = \frac{ci}{2\omega_m}\nabla_\perp^2\Omega_m + ik_{01}a_1a_0^*, \tag{4b}$$

where $k_{03(01)} = N_a\omega_{p(m)}|\mathbf{p}_{03(01)}|^2/(2\epsilon_0 c\hbar)$ are the coupling constants, N_a is the atomic density, and $\mathbf{p}_{ij}$ is the electric dipole matrix element associated with the transition from $|i\rangle$ to $|j\rangle$.

Under the weak-probe-field mechanism, we assume that most atoms will remain in the ground state $|0\rangle$, so we can choose $|a_0|^2 \approx 1$. Taking the Fourier transform of Eqs. (3) and (4), we obtain [24]

$$\beta_1 A_1 + \Omega_v A_2 + \Omega_m = 0, \tag{5a}$$

$$\beta_2 A_2 + \Omega_v^* A_1 + \Omega_a A_3 = 0, \tag{5b}$$

$$\beta_3 A_3 + \Omega_a^* A_2 + \Omega_p + \Omega_{c2}A_5 + \Omega_{c1}A_4 = 0, \tag{5c}$$

$$\beta_4 A_4 + \Omega_{c1}^* A_3 = 0, \tag{5d}$$

$$\beta_5 A_5 + \Omega_{c2}^* A_3 = 0, \tag{5e}$$

and

$$\frac{\partial F_p}{\partial z} - i\frac{\omega}{c}F_p = i\frac{c}{2\omega_p}\nabla_\perp^2 F_p + ik_{03}A_3, \tag{6a}$$

$$\frac{\partial F_m}{\partial z} - i\frac{\omega}{c}F_m = i\frac{c}{2\omega_m}\nabla_\perp^2 F_m + ik_{01}A_1, \tag{6b}$$

where $\beta_1 = \omega + \Delta_m + i\gamma_1$, $\beta_2 = \omega + \Delta_a + i\gamma_2$, $\beta_3 = \omega + \Delta_p + i\gamma_3$, $\beta_4 = \omega + \Delta_p - \Delta_{c1} + i\gamma_4$, and $\beta_5 = \omega + \Delta_p - \Delta_{c2} + i\gamma_5$. ω is the Fourier variable. $A_{i=1-5}$, F_p, and F_m are the Fourier transforms of $a_{i=1-5}$, Ω_p, and Ω_m, respectively. The first terms on the right-hand side of Eqs. (6a) and (6b) account for the transverse variations of the probe and FWM fields, which are responsible for the diffraction either in the medium or in vacuum. If the propagation distance L of the probe field or the FWM field is much less than the Rayleigh distance $z_R = \pi\omega_0^2/\lambda$, i.e., $L \ll \pi\omega_0^2/\lambda$, then the diffraction terms can be ignored [25,26]. In this work, the propagation distance of the FWM field is $L = 20$ mm, and the transverse characteristic size is beam waist $\omega_0 = 0.2$ mm. The wavelength of the FWM

field is $\lambda \approx 297$ nm; then we can obtain $\pi\omega_0^2/\lambda \approx 422.9$ nm $\gg 20$ mm, so the diffraction term can be canceled out in the following.

By solving Eq. (5), it is easy to obtain the following relations:

$$A_1 = \frac{\Omega_\nu \Omega_a \beta_4 \beta_5}{D} F_p + \frac{D_1}{D} F_m, \tag{7a}$$

$$A_3 = \frac{D_3 \beta_4 \beta_5}{D} F_p + \frac{\Omega_\nu^* \Omega_a^* \beta_4 \beta_5}{D} F_m, \tag{7b}$$

where we defined $D_1 = \beta_2\beta_3\beta_4\beta_5 - \beta_2\beta_5|\Omega_{c1}|^2 - \beta_2\beta_4|\Omega_{c2}|^2 - \beta_4\beta_5|\Omega_a|^2$, $D_2 = \beta_1\beta_2 - |\Omega_\nu|^2$, and $D = \beta_1\beta_2\beta_5|\Omega_{c1}|^2 + \beta_1\beta_2\beta_4|\Omega_{c2}|^2 + \beta_1\beta_4\beta_5|\Omega_a|^2 - \beta_5|\Omega_\nu|^2|\Omega_{c1}|^2 - \beta_4|\Omega_{c2}|^2|\Omega_\nu|^2 - \beta_1\beta_2\beta_3\beta_4\beta_5$.

Substituting Eq. (7) into Eq. (6) with the initial conditions $F_p(z=0,\omega) = \Omega_{p0}\exp(-\omega^2 \ln 2/2\pi^2)$ and $F_m(z=0,\omega) = 0$, the analytical solutions of F_p and F_m are

$$F_p(z,\omega) = \frac{U_+ e^{(iK_- z)} - U_- e^{(iK_+ z)}}{U_+ - U_-} F_p(0,\omega), \tag{8a}$$

$$F_m(z,\omega) = \frac{U_+ U_- F_p(0,\omega)}{U_+ - U_-}\left[e^{(iK_- z)} - e^{(iK_+ z)}\right], \tag{8b}$$

where $U_\pm = (k_{01}D_1 - k_{03}D_2\beta_4\beta_5 \pm G)/(2k_{03}^*\Omega_\nu^*\Omega_a^*\beta_4\beta_5)$ and $K_\pm = \omega/c + (k_{01}D_1 + k_{03}\beta_4\beta_5 D_3 \pm G)/(2D) = K_\pm(0) + \omega/V_{g\pm} + O(\omega^2)$, where $V_{g\pm} = 1/\mathrm{Re}(\partial K_\pm/\partial\omega|_{\omega=0})$ is the group velocity of the $K_\pm$ mode and $G = [(k_{01}D_1 - k_{03}\beta_4\beta_5 D_2)^2 + 4k_{01}k_{03}\beta_4^2\beta_5^2|\Omega_\nu|^2|\Omega_a|^2]^{1/2}$.

From Eqs. (8a) and (8b), one can see that there are two modes described by the dispersion relations K_+ and K_-. In the adiabatic regime [27,28], mode K_- will quickly decay around the center frequency, which can be neglected after propagating for a longer optical depth. Then, the inverse Fourier transform of F_m and F_p can be written as

$$\Omega_p(z,t) = \frac{U_-}{U_- - U_+}\Omega_p(\eta_+)e^{iK_+ z}, \tag{9a}$$

$$\Omega_m(z,t) = \frac{U_+ U_-}{U_- - U_+}\Omega_p(\eta_+)e^{iK_+ z}, \tag{9b}$$

where $\eta_+ = t - z/V_{g+}$.

Finally, the generated FWM field after a propagation distance L can be given as

$$\Omega_m(L,t) = \tilde{\Omega}_m e^{-i\phi l} e^{iLK_+}, \tag{10}$$

where $\tilde{\Omega}_m = k_{01}\Omega(r)\Omega_{\nu 0}\Omega_a\Omega_p(\eta_+)\beta_4\beta_5/G$. From Eq. (10), we find the FWM field $\Omega_m(L,t) \sim e^{-il\phi}$ is generated with the same vorticity as the OAM field $\Omega_\nu \sim e^{-il\phi}$, which implies the OAM phase of field Ω_ν is entirely transferred to the FWM field.

Using $K_+ = \mathrm{Re}(K_+) + i\mathrm{Im}(K_+)$, we can rewrite Eq. (10) as

$$\Omega_m(L,t) = \tilde{\Omega}_m e^{-L\mathrm{Im}(K_+)} e^{-i[\phi l - L\,\mathrm{Re}(K_+)]}, \tag{11}$$

where the intensity of the FWM field is $\propto |\tilde{\Omega}_m e^{-L\mathrm{Im}(K_+)}|^2$, while the factor $e^{-i[\phi l - L\mathrm{Re}(K_+)]}$ reflects the phase of the FWM field.

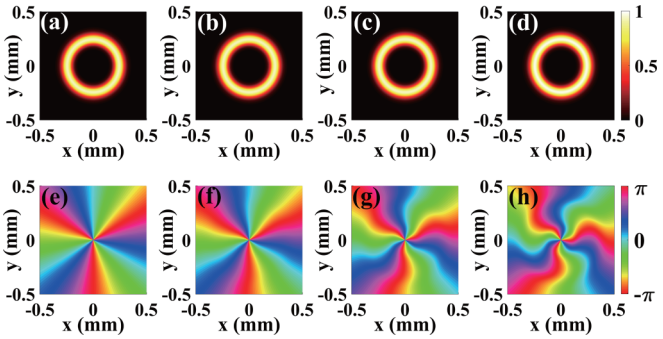

FIG. 2. Normalized intensity patterns of the FWM field for different values of the control field Ω_{c1}: (a) $\Omega_{c1} = 1$ MHz, (b) $\Omega_{c1} = 10$ MHz, (c) $\Omega_{c1} = 20$ MHz, and (d) $\Omega_{c1} = 30$ MHz. (e)–(h) Corresponding phase patterns of the FWM field. The parameters are $\Omega_{c2} = 10$ MHz, $\Omega_{\nu 0} = 3$ MHz, $\omega_0 = 0.2$ mm, $\omega_{sp} = 3\omega_0$, $l = 3$, $p = 0$, $\Delta_p = 10$ MHz, $\Delta_a = \Delta_m = 0$, $\Delta_{c1} = -2$ MHz, $\Delta_{c2} = 1$ MHz, $\Omega_a = 10\sqrt{2}$ MHz, $\gamma_1 = 0.09$ MHz, $\gamma_2 = 0.8$ MHz, $\gamma_3 = 5.9$ MHz, $\gamma_4 = \gamma_5 = 0$, $L = 2$ cm, $\Omega_{p0} = 1$ MHz, $k_{01} = 10^9$ m^{-1}s^{-1}, $k_{03} = 10^{11}$ m^{-1} s^{-1}.

III. RESULTS AND DISCUSSION

In Fig. 2, we illustrate the intensity distribution as well as the phase pattern profiles of the generated FWM field described by Eq. (11) for different values of the control field Ω_{c1}. As shown in Figs. 2, the intensity distribution remains unchanged and shows a doughnut pattern, while the phase pattern becomes twisted. Actually, states $|0\rangle$, $|3\rangle$, and $|4\rangle$ construct a standard EIT system. By tuning the intensity of the control field Ω_{c1}, the linear and nonlinear responses of the atomic medium can be easily controlled, which results in the different findings in Fig. 2. In order to inspect the influence of the control field Ω_{c1} on the FWM field, we plot the real part $\mathrm{Re}(K_+)$ and imaginary part $\mathrm{Im}(K_+)$ of the dispersion relation K_+ versus radius r for different values of the control field Ω_{c1} in Fig. 3. As illustrated in Fig. 3(a), as the control field Ω_{c1} increases, the influence of the control field Ω_{c1} on the imaginary part $\mathrm{Im}(K_+)$ is weak, so the change in the intensity distribution is very limited in Figs. 2(a)–2(d). In contrast, by increasing the control field Ω_{c1}, the real part $\mathrm{Re}(K_+)$ increases remarkably [see Fig. 3(b)], which means that the spatial dependency of the phase is increasing. So we can see the phase patterns become twisted in Figs. 2(f)–2(h).

Figure 4 shows the effect of the control field Ω_{c2} on the FWM field. From this figure, we can see that the intensity distributions and the phase patterns are very similar to the profiles displayed in Figs. 2. Clearly, the control field Ω_{c2} can also be used to modulate the phase of the FWM field. In order to understand the above phenomena, again we display the real part $\mathrm{Re}(K_+)$ and imaginary part $\mathrm{Im}(K_+)$ of the dispersion relation K_+ versus radius r for different values of control field Ω_{c2} in Fig. 5. The resulting curves of the imaginary part $\mathrm{Im}(K_+)$, shown in Fig. 5(a), confirm that the intensity distribution is nearly independent of the control field Ω_{c2} in Figs. 4(a)–4(d). Yet with changing the control field Ω_{c2}, the real part $\mathrm{Re}(K_+)$ varies significantly in Fig. 5(b), causing the twisted phase patterns in Figs. 4(f)–4(h).

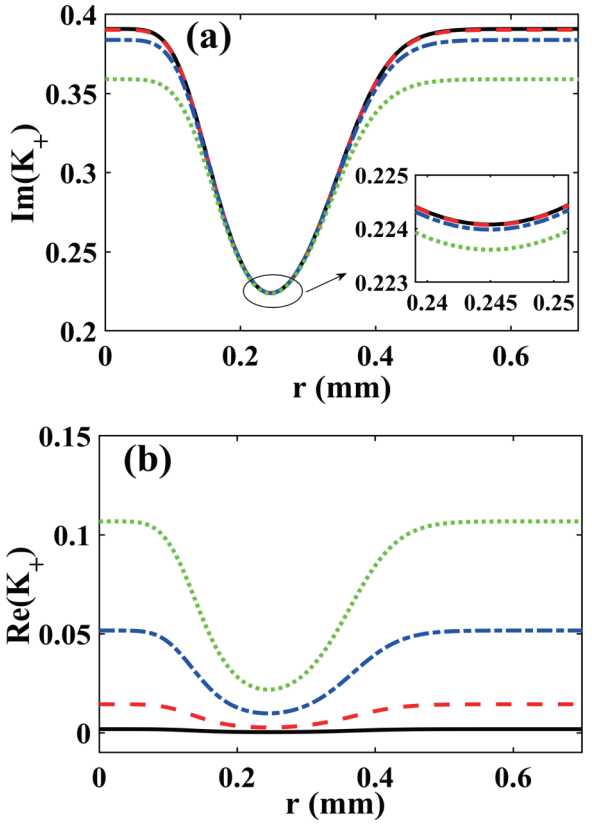

FIG. 3. The (a) imaginary and (b) real parts of the dispersion relation K_+ versus radius r for different values of the control field Ω_{c1}: Solid line, $\Omega_{c1} = 1$ MHz; dashed line, $\Omega_{c1} = 10$ MHz; dot-dashed line, $\Omega_{c1} = 20$ MHz; and dotted line, $\Omega_{c1} = 30$ MHz. The inset in (a) shows the minima of $\mathrm{Im}(K_+)$. Other parameters are the same as in Fig. 2.

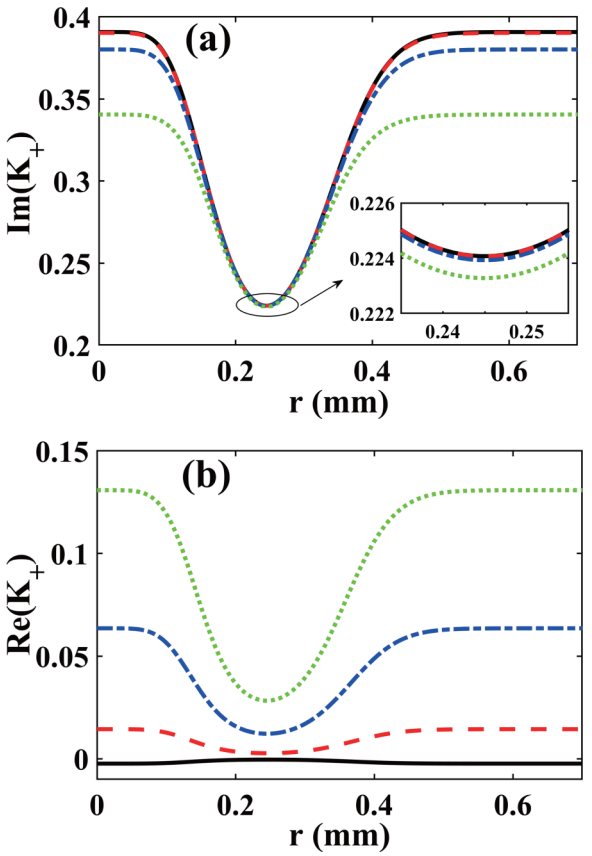

FIG. 5. The (a) imaginary and (b) real parts of the dispersion relation K_+ versus radius r for different values of the control field Ω_{c2}: Solid line, $\Omega_{c2} = 1$ MHz; dashed line, $\Omega_{c2} = 10$ MHz; dot-dashed line, $\Omega_{c2} = 20$ MHz; and dotted line, $\Omega_{c2} = 30$ MHz. The inset in (a) shows the minima of $\mathrm{Im}(K_+)$. Other parameters are the same as in Fig. 4.

We note that, very recently, a theoretical scheme for controlling the space-dependent FWM in a four-level atomic system was proposed [29]. In that scheme, a four-level atomic system was used to manipulate the FWM via the intensity of a control field. In comparison with that scheme, the major features of our proposal are the following. First, the main difference between our scheme and the one in [29] is that we have utilized the double-dark resonance induced by two additional control beams, Ω_{c1} and Ω_{c2}, while in [29] only a single-dark resonance (i.e., conventional EIT) is used. The double-dark resonance scheme has many advantages for controlling the FWM in comparison with the single-dark

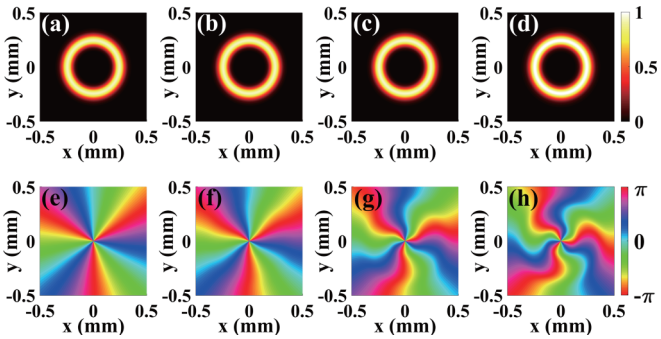

FIG. 4. Normalized intensity patterns of the FWM field for different values of the control field Ω_{c2}: (a) $\Omega_{c12} = 1$ MHz, (b) $\Omega_{c2} = 10$ MHz, (c) $\Omega_{c2} = 20$ MHz, and (d) $\Omega_{c2} = 30$ MHz. (e)–(h) Corresponding phase patterns of the FWM field. Other parameters are the same as in Fig. 2 except for $\Omega_{c1} = 10$ MHz.

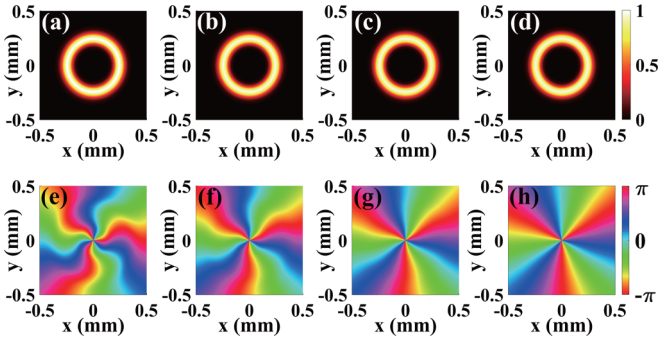

FIG. 6. Normalized intensity patterns of the FWM field for different values of the probe detuning Δ_p: (a) $\Delta_p = 3$ MHz, (b) $\Delta_p = 6$ MHz, (c) $\Delta_p = 10$ MHz, and (d) $\Delta_p = 15$ MHz. (e)–(h) Corresponding phase patterns of the FWM field. Other parameters are the same as in Fig. 2 except for $\Omega_{c1} = \Omega_{c2} = 10$ MHz.

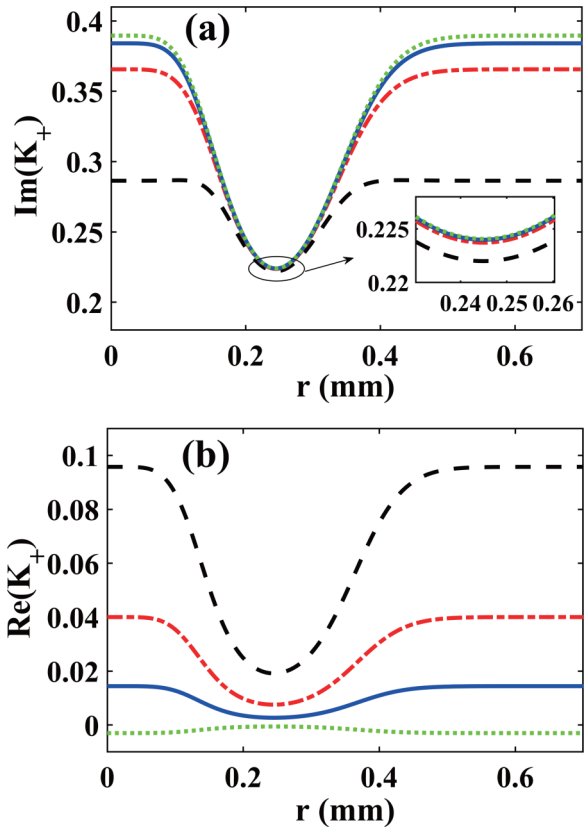

FIG. 7. The (a) imaginary and (b) real parts of the dispersion relation K_+ versus radius r for different values of the probe detuning Δ_p: Dashed line, $\Delta_p = 3$ MHz; dot-dashed line, $\Delta_p = 6$ MHz; solid line, $\Delta_p = 10$ MHz; and dotted line, $\Delta_p = 15$ MHz. The inset in (a) shows the minima of $\mathrm{Im}(K_+)$. Other parameters are the same as in Fig. 6.

resonance one. For example, the double-dark resonance provides two transparency windows, and in different windows the spatial variations of the FWM are different. Second, in the double-dark resonance scheme more physical parameters (e.g., the control fields Ω_{c1} and Ω_{c2}) can be manipulated, and hence, one can select suitable parameters to explore singularity characteristics of the helical phase wave front in nonlinear processes. Third, with increasing the control field Ω_{c1} or control field Ω_{c2}, intensity distribution remains unchanged, but the phase pattern is twisted. The findings are quite different from the results obtained in [29], where the FWM field is enhanced and phase twist is almost completely suppressed by increasing the control field.

Finally, we present the intensity distribution and the phase pattern of the FWM field for different values of the probe detuning Δ_p in Fig. 6. Figure 6 shows that the FWM field has an intensity distribution independent of the probe detuning Δ_p, yet the singularity variation appears obviously in phase patterns, indicating that spatially varying dispersion is almost completely suppressed with increasing detuning of the probe field Δ_p. Also, the real part $\mathrm{Re}(K_+)$ and imaginary part $\mathrm{Im}(K_+)$ of the dispersion relation K_+ versus radius r for different values of the probe detuning Δ_p are illustrated in Fig. 7. As we expected, by increasing the probe field Δ_p, the imaginary part changes limitedly, while the real part increases remarkably. In fact, one can see from Figs. 6 and 7 that, in comparison with the results in [15–17,29], where the increasing detuning leads to phase twist, we can effectively suppress phase twist via the increasing detuning of the probe field Δ_p in our present six-level tripod scheme. Here, it should be emphasized that the above description may provide a clue for engineering the helical phase wave front by properly adjusting the probe detuning, which could potentially be used to engineer the helical phase profile, such as helical phase reconstruction and helical phase purification.

IV. CONCLUSION

In conclusion, we proposed a theoretical scheme to manipulate the helical phase via ultraslow four-wave mixing in a six-level atomic system driven by a field with OAM and making use of two EIT control fields. It was found that the FWM field has stable intensity distribution independent of the corresponding system parameters. More interestingly, one can effectively control the helical phase of the output FWM field via the intensities of the two EIT control fields as well as the detuning of the probe field. As a result, the phase engineering proposed here has the potential for various applications in the transfer of OAM [30], storage of OAM [31], high-helicity OAM conversion [32], and the generation of OAM entanglement [33,34].

ACKNOWLEDGMENTS

Z.W. acknowledges financial support from the National Natural Science Foundation of China (Grant No. 11674002).

[1] M. Xiao, Y. Q. Li, S. Z. Jin, and J. Gea-Banacloche, Phys. Rev. Lett. **74**, 666 (1995).
[2] S. E. Harris, Phys. Today **50**(7), 36 (1997).
[3] M. Fleischhauer, A. Imamoglu, and J. P. Marangos, Rev. Mod. Phys. **77**, 633 (2005).
[4] Y.-Q. Li and M. Xiao, Opt. Lett. **21**, 1064 (1996).
[5] L. Deng, M. Kozuma, E. W. Hagley, and M. G. Payne, Phys. Rev. Lett. **88**, 143902 (2002).
[6] Y. Wu, J. Saldana, and Y. Zhu, Phys. Rev. A **67**, 013811 (2003).
[7] Y. Niu, R. Li, and S. Gong, Phys. Rev. A **71**, 043819 (2005).
[8] Y. Zhang, U. Khadka, B. Anderson, and M. Xiao, Phys. Rev. Lett. **102**, 013601 (2009).
[9] L. Allen, M. W. Beijersbergen, R. J. C. Spreeuw, and J. P. Woerdman, Phys. Rev. A **45**, 8185 (1992).
[10] M. Padgett, J. Courtial, and L. Allen, Phys. Today **57**(5), 35 (2004).
[11] J. W. R. Tabosa and D. V. Petrov, Phys. Rev. Lett. **83**, 4967 (1999).
[12] A. M. Akulshin, R. J. McLean, E. E. Mikhailov, and I. Novikova, Opt. Lett. **40**, 1109 (2015).

[13] Z. Zhang, D. Ma, Y. Zhang, M. Cao, Z. Xu, and Y. Zhang, Opt. Lett. **42**, 1059 (2017).
[14] N. Prajapati, N. Super, N. R. Lanning, J. P. Dowling, and I. Novikova, Opt. Lett. **44**, 739 (2019).
[15] Y. Hong, Z. Wang, D. Ding, and B. Yu, Opt. Express **27**, 29863 (2019).
[16] Y. Zhang, Z. Wang, J. Qiu, Y. Hong, and B. Yu, Appl. Phys. Lett. **115**, 171905 (2019).
[17] J. Qiu, Z. Wang, D. Ding, W. Li, and B. Yu, Opt. Express **28**, 2975 (2020).
[18] M. D. Lukin, S. F. Yelin, M. Fleischhauer, and M. O. Scully, Phys. Rev. A **60**, 3225 (1999).
[19] E. Paspalakis and P. L. Knight, Phys. Rev. A **66**, 015802 (2002).
[20] R. Mukherjee, C. Ates, W. Li, and S. Wüster, Phys. Rev. Lett. **115**, 040401 (2015).
[21] C. Muldoon, L. Brandt, J. Dong, D. Stuart, E. Brainis, M. Himsworth, and A. Kuhn, New J. Phys. **14**, 073051 (2012).
[22] N. Radwell, T. W. Clark, B. Piccirillo, S. M. Barnett, and S. Franke-Arnold, Phys. Rev. Lett. **114**, 123603 (2015).
[23] M. O. Scully and M. S. Zubairy, *Quantum Optics* (Cambridge University, Cambridge, 1997).
[24] Y. Wu, M. G. Payne, E. W. Hagley, and L. Deng, Opt. Lett. **29**, 2294 (2004).
[25] H. R. Hamedi, E. Paspalakis, G. Zlabys, G. Juzeliunas, and J. Ruseckas, Phys. Rev. A **100**, 023811 (2019).
[26] H. R. Hamedi, J. Ruseckas, E. Paspalakis, and G. Juzeliunas, Phys. Rev. A **101**, 063828 (2020).
[27] Y. Wu and X. Yang, Phys. Rev. A **70**, 053818 (2004).
[28] H. J. Li and G. Huang, Phys. Rev. A **76**, 043809 (2007).
[29] J. Qiu, Z. Wang, D. Ding, Z. Huang, and B. Yu, Phys. Rev. A **102**, 033516 (2020).
[30] G. Walker, A. S. Arnold, and S. Franke-Arnold, Phys. Rev. Lett. **108**, 243601 (2012).
[31] D. S. Ding, W. Zhang, Z. Y. Zhou, S. Shi, G. Y. Xiang, X. S. Wang, Y. K. Jiang, B. S. Shi, and G. C. Guo, Phys. Rev. Lett. **114**, 050502 (2015).
[32] A. Chopinaud, M. Jacquey, B. Viaris de Lesegno, and L. Pruvost, Phys. Rev. A **97**, 063806 (2018).
[33] X. Pan, S. Yu, Y. Zhou, K. Zhang, K. Zhang, S. Lv, S. Li, W. Wang, and J. Jing, Phys. Rev. Lett. **123**, 070506 (2019).
[34] K. Zhang, W. Wang, S. Liu, X. Pan, J. Du, Y. Lou, S. Yu, S. Lv, N. Treps, C. Fabre, and J. Jing, Phys. Rev. Lett. **124**, 090501 (2020).